PCCP

Difference between approximate and rigorously measured transference numbers in fluorinated electrolytes

Journal:	*Physical Chemistry Chemical Physics*
Manuscript ID	CP-ART-01-2019-000216.R2
Article Type:	Paper
Date Submitted by the Author:	19-Mar-2019

Complete List of Authors:	Shah, Deep; University of California Berkeley Research, Chemical and Biomolecular Engineering Nguyen, Hien; University of California, Berkeley, Department of Chemical and Biomolecular Engineering Grundy, Lorena; University of California, Berkeley, Department of Chemical and Biomolecular Engineering Olson, Kevin; University of North Carolina at Chapel Hill, Chemistry Mecham, Sue; University of North Carolina at Chapel Hill, Chemistry Desimone, J.; University of North Carolina, Department of Chemistry Balsara, Nitash; University of California, Chemical and Biomolecular Engineering

Difference between approximate and rigorously measured transference numbers in fluorinated electrolytes

Deep B. Shah,[a,b] Hien Q. Nguyen,[a] Lorena S. Grundy,[a] Kevin R. Olson,[c] Sue J. Mecham,[c] Joseph M. DeSimone,[c,d] and Nitash P. Balsara[a,b,e,*]

[a] Department of Chemical and Biomolecular Engineering, University of California, Berkeley, CA 94720, USA

[b] Materials Science Division, Lawrence Berkeley National Laboratory, Berkeley, CA 94720, USA

[c] Department of Chemistry, University of North Carolina at Chapel Hill, Chapel Hill, North Carolina 27599, USA

[d] Department of Chemical and Biomolecular Engineering, North Carolina State University, Raleigh, North Carolina 27695, USA

[e] Energy Storage and Distributed Resources Division, Lawrence Berkeley National Laboratory, Berkeley, CA 94720, USA

Corresponding Author:

[*] Nitash P. Balsara: E-mail: nbalsara@berkeley.edu, Address: Department of Chemical Engineering, 201 Gilman Hall, University of California, Berkeley, CA 94720-1462, USA, Phone: (+1) 510-642-8973.

Abstract

The performance of binary electrolytes is governed by three transport properties: conductivity, salt diffusion coefficient, and transference number. Rigorous methods for measuring conductivity and the salt diffusion coefficient are well established and used routinely in the literature. The commonly used methods for measuring transference number are the steady-state current method, $t_{+,id}$, and pulsed field gradient NMR, $t_{+,NMR}$. These methods yield the transference number only if the electrolyte is ideal, i.e., the salt dissociates completely into non-interacting anions and cations. In this work, we present a complete set of ion transport properties for mixtures of a functionalized perfluoroether, dimethyl carbonate terminated perfluorinated tetraethylene ether, and lithium bis(fluorosulfonyl)imide (LiFSI). The equations used to determine these properties from experimental data are based on Newman's concentrated solution theory. The concentrated-solution-theory-based transference number, t_+^0, is negative across all salt concentrations, and it increases with increasing salt concentration. In contrast, the ideal transference number, $t_{+,id}$, is positive across all salt concentrations and it decreases with salt concentration. The NMR-based transference number, $t_{+,NMR}$, is approximately 0.5, independent of salt concentration. The disparity between the three transference numbers, which indicates the dominance of ion clustering, is resolved by the use of Newman's concentrated solution theory.

Keywords

Transference number, Li ion transport, PFG-NMR, Perfluoropolyether, Perfluoroether

1. Introduction

Developing next generation lithium-ion technology requires synergistic efforts ranging from electrode development to electrolyte engineering. Electrolytes used in current lithium-ion cells are typically mixtures of ethylene carbonate (EC), dimethyl carbonate (DMC) and lithium hexafluorophosphate ($LiPF_6$).[1-4] However, these electrolytes are highly flammable at room temperature; the flash point of DMC is 18 °C. The development of nonflammable electrolytes has thus garnered considerable attention. Electrolytes based on fluorinated solvents have been recently shown as interesting candidate materials for lithium-ion batteries.[5-10] While fluorinated additives are often used in lithium-ion technology to help stabilize the solid electrolyte interphase layer at the anode, the notion that a fluorinated solvent could serve as an electrolyte is relatively new.[11,12] These electrolytes exhibit larger electrochemical stability windows than alkyl carbonates.[9] The standard approach for quantifying ion transport in electrolytes comprises measurement of ionic conductivity, κ, using blocking electrodes. However, it is well established that complete characterization of a binary electrolyte (solvent + salt) requires measurement of two additional transport coefficients, the salt diffusion coefficient, D, and the transference number of the cation with respect to the velocity of the solvent, , t_+^0, and the thermodynamic factor, T_f.[13,14]

The transference number of fluorinated electrolytes is of interest due to fundamental differences in solvent-salt interactions relative to conventional electrolytes. In conventional electrolytes such as alkyl carbonates, the salt-solvent interactions are dominated by associations between oxygen atoms on the solvent and lithium cations. Such associations are weakened in fluorinated electrolytes due to the electron withdrawing character of fluorine atoms. Instead, one might

expect associations between the fluorinated solvent and the fluorinated anion due to the well-documented fluorous effect.[15,16] These interactions could result in an increase in the cation transference number, which, in turn, could improve the efficacy of fluorinated electrolytes. Interestingly, reported cation transference numbers of fluorinated electrolytes in the literature are as high as 0.9, compared with 0.4 or less in conventional electrolytes.[6,7,17-19] All of the cation transference numbers of fluorinated electrolytes reported in the literature are based on the assumption that the solutions are ideal. An ideal electrolyte is defined to be one that contains completely disassociated ions that do not interact with each other and this gives rise to activity coefficients that are unity and independent of molality. We use a symbol $t_{+,id}$ to refer to the transference number based on the ideal solution approximation. The method for measuring $t_{+,id}$ was pioneered by Bruce and Vincent.[20,21] The high ideal cation transference number is often taken as a signature of rapid diffusion of the cation relative to the anion. A standard approach for measuring the self-diffusion coefficient of the ions is pulsed field gradient NMR (PFG-NMR).[22-26] If the ideal solution assumption were valid, then $t_{+,NMR}$ and $t_{+,id}$ would be in quantitative agreement.

The purpose of this paper is to report on the complete electrochemical characterization of a fluorinated electrolyte including measurement of κ, D, t_+^0 and T_f. The chemical structures of the fluorinated solvent, C8-DMC, is shown in Figure 1a and that of the FSI anion is shown in Figure 1b. Pulsed field gradient NMR experiments were used to quantify self-diffusion coefficients of the cations and anions in this fluorinated electrolyte. We show that the rigorously measured transference number, t_+^0, differs qualitatively from that obtained using the ideal solution approximation.

2. Experimental Details

2.1 Perfluoroether Synthesis

The perfluoroether (PFE) was synthesized from a diol terminated precursor following procedures described in Wong, D. *et al.* and Olson, K. *et al*.[8,27] Figure 1a shows our approach to synthesize C8-DMC. 0.10 mol of the perfluorinated glycol precursor (0.20 mol -OH end groups) and three molar equivalents triethylamine (84 mL, 0.60 mol) were dissolved in 400 mL of 1,1,1,3,3-pentafluorobutane in a 1 L 3-neck round-bottom flask. The solution was cooled to 0°C under nitrogen atmosphere using a salt + ice bath. Methyl chloroformate (46 mL, 0.60 mol) was added dropwise over the course of two hours with rapid stirring, resulting in significant gas evolution and formation of the white triethylamine hydrochloride (TEA HCl) precipitate. The reaction was stirred overnight under nitrogen atmosphere at ambient temperature, and reaction completion was confirmed by proton nuclear magnetic resonance (^{1}H-NMR).

The TEA HCl salt was removed by gravity filtration, yielding a pale-yellow solution. The salt was washed three times with 50 mL 1,1,1,3,3-pentafluorobutane to remove residual product. The combined pentafluorobutane solution was then washed 3x with 500 mL water and 1x with 500 mL brine using a separatory funnel. The solution was stirred with activated carbon to remove coloration and dried with magnesium sulfate. After filtering the solids, pentafluorobutane was removed under reduced pressure, yielding a clear oil. The dimethyl carbonate terminated perfluorinated tetraethylene ether (C8-DMC) was dried under vacuum at 50°C for two days. The molecular weight (MW) for C8-DMC is 526 g/mol. Figures S1a and S1b in the supplemental information show the ^{1}H-NMR spectra of the precursor and product dissolved in deuterated acetone.

Thermogravimetric analysis (TGA) was used to determine the volatility of C8-DMC using a TA Instruments Q5000 TGA under nitrogen flow (10 mL/min) from 25 °C to 500 °C at a heating rate of 10 °C/min. The temperature at which a 5% mass loss were recorded from the TGA curve was 129 °C for C8-DMC. Closed-cup flash point measurements were performed using an Erdco Rapid Tester small-scale apparatus following ASTM D 3278. No flash point was detected for C8-DMC within the experimental window (up to 250°C).

2.2 Salts

Lithium bis(fluorosulfonyl)imide (LiFSI) (cat. no. 097602) was purchased from Oakwood Products, Inc. The salt was ≥ 99% pure, as confirmed by a Certificate of Analysis form. The salt was dried at 100 °C under dynamic vacuum for three days inside a glovebox antechamber. The salt, oligomer, and electrolytes were stored within an argon filled Vac glovebox with H_2O and O_2 concentrations kept below 1 ppm.

2.3 Electrolyte Preparation

Prior to transfer into the glovebox, C8-DMC was dried under active vacuum inside the glovebox antechamber at 50 °C for 72 hours. In order to form electrolytes, a predetermined amount of Li salt was added to a known mass of C8-DMC. Once the salt was added, the electrolytes were placed on a magnetic stirrer and were allowed to mix for 12 hours or more using a magnetic stir bar.

2.3 Experimental Characterization

All experiments were conducted at 30 °C ± 1 °C. Coin cells were run in heating ovens and concentration cells were immersed in a temperature controlled oil bath. All the error bars reported are standard deviations of replicate measurements. Error propagation formulas for relevant measurements are reported in supplemental information.

Conductivity measurements

Conductivity samples were prepared by sandwiching an electrolyte soaked separator, Celgard 2500 (Celgard Company), with a stainless steel shim (MTI Corporation) on either side. The stainless steel shims were 15.5 mm in diameter and 0.2 mm in thickness; Celgard 2500 was cut to 19 mm in diameter and had a thickness of 25 μm. The stack was placed into CR2032 coin cells (Pred Materials) that were than hermetically sealed. Three replicate cells were produced and measured for each electrolyte. Conductivity data was collected through ac impedance spectroscopy performed on a Bio-Logic VMP3 potentiostat. The frequency range analyzed was between 1 MHz and 100 mHz at an amplitude of 60 mV. Figure 2a shows typical impedance data collected in coin cells and the equivalent circuit is shown in the inset. Here, R_s is the resistance of the electrolyte/separator composite, Q and Q_{int} are the constant phase elements associated with the electrolyte/separator and interface, respectively, and R_c and L_c are the resistance and inductance, respectively, associated with the VMP3 cables. The conductivity of the electrolytic phase, κ, was calculated using Equation 1

$$\kappa = \frac{\tau \quad l}{\phi_c R_s A} \tag{1}$$

where A is the electrode area of the coin cells in cm^2, l is the thickness of the separator in cm, τ is the tortuosity of the separator and ϕ_c is the volume fraction of the conducting element within the separator. Both τ and ϕ_c are experimentally determined, and the ratio was determined by measuring the conductivity of five electrolytes using a FiveEasy Conductivity Meter F30 (Mettler Toledo) and dividing the obtained conductivity values by the separator conductivities. The five molalities measured using the conductivity probe were 0.28, 0.60, 0.94, 1.30 and 1.78 mol LiFSI/kg C8-DMC and $\frac{\tau}{\phi_c}$ was found to be 8.47 ± 0.69.

The conductivity of neat C8-DMC solvent was measured to be 3.02 x 10^{-7} S/cm, which we assume is due to impurities. We treat this value as a background and report the conductivity of our electrolytes after subtracting 3.02 x 10^{-7} S/cm from the measured values.

The cell constant, $\frac{\tau}{\phi_c}$, is also known as the MacMullin number, N_m

$$N_m = \frac{\tau}{\phi_c} = \frac{\kappa}{\kappa_s} \quad (2)$$

where κ_s is the separator conductivity.[28] The volume fraction was calculated following a similar procedure to that of reference 29. In order to calculate the porosity of the Celgard 2500 separator, 5 replicate uptake volume measurements for each salt molality were done. The average conducting phase volume fraction was found to be 0.535 ± 0.030 across the range of salt molalities. The density, ρ, at each salt concentration was obtained by filling a differential scanning calorimetry (DSC) sample pan (TA Instruments) with a known volume of 40 uL and measuring the mass of the electrolyte at 30 °C; three replicates were measured at each salt concentration. Results are shown in Table 1.

The MacMullin number was combined with the conducting phase volume fraction in order to calculate the separator tortuosity, $\tau = 4.53 \pm 0.45$.

Lithium symmetric cells for ideal transference number

Lithium symmetric cells were assembled similar to conductivity samples. However, instead of stainless steel shims, lithium discs, cut from lithium chips (MTI Corp.), were used on either side of the electrolyte-soaked Celgard. The diameter of the 150 μm thick Li disc was 12.7 mm. Three replicate cells were produced for each electrolyte. Data were collected on a Bio-Logic VMP3 potentiostat. Each sample cell was subjected to a conditioning treatment, which consisted of charge and discharge cycles at 0.02 mA/cm^2 in order to help stabilize the interfacial layer. The sequence performed was a 4 hour charge, 30 minutes rest, a 4 hour discharge, 30 minutes rest, and repeated for a total of 6 times. Ac impedance was carried out before the beginning of conditioning, after each rest step, and at the end of conditioning. Each sample was then polarized at $\Delta V = \pm$ 40 mV and ± 80 mV for 1 hour in order to ensure that the ideal transference number, $t_{+,id}$, collected was independent of the applied potential, an important consideration since the method assumes that minimal concentration gradients develop over the course of the measurement. During chronopotentiometry, current was measured at 1 second intervals in order to capture the full current response. Ac impedance data were collected every 20 minutes with an ac amplitude of 20 mV and 40 mV for the dc applied potentials of ± 40 mV and ± 80 mV, respectively. The data obtained for all of these cases were similar. We report data acquired using ac impedance spectroscopy with an amplitude of 20 mV during dc polarization of 40 mV in Figure 2b. Data were modeled to the equivalent circuit shown in the inset of Figure 2b, where

R_{int} was the interfacial resistance. Figure 2b represents the typical impedance data seen for Li symmetric cells.

Assuming Ohm's law, which is a reasonable assumption prior to cell polarization due to a lack of concentration gradients, an initial current, I_Ω, is given by Equation 3:

$$I_\Omega = \frac{\Delta V}{R_T} \tag{3}$$

where ΔV is the applied polarization potential and R_T is the total initial cell resistance as measured by ac impedance spectroscopy. Equation 4 was then used to calculate the ideal transference number:[20,30]

$$t_{+,id} = \frac{I_{ss}}{I_\Omega}\left(\frac{\Delta V - I_\Omega R_{i,0}}{\Delta V - I_{ss} R_{i,ss}}\right) \tag{4}$$

where I_{ss} is the steady state current, R_0 is the initial interfacial resistance, and R_{ss} is the interfacial resistance when I_{ss} is reached.

Restricted diffusion measurements

Diffusion coefficients were measured using the restricted diffusion technique.[28,29] Lithium electrodes (thickness 150 μm, diameter 12.7 mm) sandwiched electrolyte soaked Celgard 2500 separators (thickness 25 μm). Four dc potentials, ±40 mV and ±80 mV, were used to polarize the cell until a steady-state current was realized. The potential was then removed and the cells were allowed to relax for 2 hours while the open-circuit potential, U, was measured every 5 seconds. Porous separators were used in order to control for convection, an important precaution for liquid electrolytes.[30] Three configurations were used, with 5, 10 and 15 separators stacked to adjust the

thickness of the electrolyte. The three thicknesses, combined with four dc potentials resulted in 36 independent diffusion coefficient measurements for each salt concentration. The open circuit relaxation potential was analyzed, and representative relaxation profiles for m = 0.60 mol/kg can be seen in Figure 3 for all three electrolyte thicknesses. The relaxation profiles were fit to Equation 5

$$U(t) = k_0 + ae^{-bt} \quad (5)$$

where a and b are fit parameters and k_0 is an empirically determined offset voltage. The salt diffusion coefficient within the separator, D_s, is related to b by

$$D_s = \frac{L^2 b}{\pi^2} \quad (6)$$

where L is the thickness of the separator stack. The lower time limits of the fits are such that $\alpha = D_s t/L^2 > 0.05$.[33]

This paper reports the diffusion coefficient of the salt in the electrolytic phase, D, and in order to do so, the tortuosity of the separator had to be taken into consideration:

$$D = \tau D_s \quad (7)$$

where D_s is the measured diffusion coefficient within the separator.

Concentration cells

In order to gather information on the electrolytes' thermodynamic factor, concentration cells were made. A U-cell design, similar to what is found in Stewart et al., was custom made by Adams & Chittenden.[32] A porous glass frit separated the two sides of the U-cell, and care was taken to ensure that mixing did not occur between the two halves. Two glass frits of different pore size were used: one with pore sizes ranging from 10 – 16 μm and another ranging from 1.0

– 1.6 μm. One side of the U-cell contained a reference electrolyte of m_{ref} = 0.60 mol/kg, while the other side was filled with electrolytes of varying molalities. Both sides of the U-cell were filled with electrolyte such that the heights on both sides were the same, an effort necessary to minimize pressure differences across the glass frit. Strips of lithium (MTI Corp.) were cut and brushed, and then immersed into the two halves of the U-cell. The open-circuit potential, U, was monitored with time. The open-circuit potential was monitored for 1 hour, in which the potential plateaued for the entirety of the measurement, further confirming that electrolyte mixing did not occur within the measurement time frame. The potential difference is related to the thermodynamic factor by the following equation:[13]

$$\frac{F(z^+ v^+)}{vRT(1-t_+^0)}\frac{dU}{dlnm} = 1 + \frac{dln\gamma_\pm}{dlnm} \quad (8)$$

where z^+ is the charge number, v^+ is the number of cations, both of which are 1 for LiFSI, and $\frac{dU}{d\ln m}$ is the change in the open-circuit potential, U, with ln(m).

Transference number calculation

The transference number of the electrolytic phase, t_+^0, was then calculated by combining the above four independent measurements (conductivity, ideal transference number, concentration cells, and restricted diffusion). Balsara and Newman showed that the ideal transference number is related to the cation transference number[35]

$$t_+^0 = 1 - \sqrt{\frac{\frac{F^2\phi_c D_s c}{v\kappa_s RT}\left(\frac{1}{t_{+,id}} - 1\right)}{1 + \frac{dln\gamma_\pm}{dlnm}}}. \quad (9)$$

Here, v is related to the stoichiometric factor and is equal to 2 for a monovalent salt. The volume fraction of the conducting phase, ϕ_c, must also be included if the separator conductivity, κ_s, and

separator salt diffusion coefficient, D_s, are used since t_+^0 is a property of only the electrolytic phase. By combining Equation 9 with Equation 8, the thermodynamic factor can be determined with experimentally measurable quantities

$$\frac{\kappa_s(z^+ v^+)}{vRT\phi_c D_s c\left(\frac{1}{t_{+,id}} - 1\right)}\left(\frac{dU}{dlnm}\right)^2 = 1 + \frac{dln\gamma_{\pm}}{dlnm}. \quad (10)$$

Equation 10 is slightly different from similar equations used by us to analyze data.[36,37] The main difference is that the $\frac{dU}{\mathrm{d}\ln m}$ term in Equation 10 is squared. The sign of the open circuit potential depends on convention – some researchers report positive values for U, while others report negative values for U.[32,35-37] This depends on whether the positive or negative lead from the potentiostat is connected to the reference electrolyte. Equation 10 is applicable regardless of convention or how the potentiostat is connected to the reference electrolyte. Once the thermodynamic factor is calculated, t_+^0 can be determined. Additionally, the above equation is true for all concentrations, as there are no assumptions about ideality within the calculation of t_+^0.

Pulsed field gradient NMR

NMR samples were prepared in an argon glovebox using 5 mm tubes with high-pressure caps. Self-diffusion coefficients were measured on a Bruker Avance 600 MHz instrument with a Z-gradient direct detection broad-band probe and a variable temperature unit maintained at 30 °C throughout the experiments. Measurements were performed on ^{7}Li at 233 MHz and ^{19}F at 565 MHz to probe the diffusion of the lithium cations and fluorine-containing FSI anions. The peak at 50 ppm is assigned to the FSI anion (see Figure S2a and S2b in supplemental information). The T_1 of each peak was measured using inversion recovery, and a recycle delay of at least 4

times T_1 was used in diffusion measurements. For all samples containing less than m = 1.30 mol/kg, a double stimulated bipolar gradient pulse sequence (Bruker sequence dstebpgp3s) was used to correct for convection in the sample.[39,40] Because of the lower signal intensity in more concentrated electrolytes, a longitudinal delay eddy current delay without convection compensation was used (Bruker sequence stebpgp1s). Experiments were performed with a variety of diffusion delays and pulse lengths to confirm that convection was not a source of inaccuracy in these samples. Diffusion intervals, Δ, varied from 0.5 to 1 s (^{7}Li) and 0.07 to 0.15 s (^{19}F), and pulse lengths, δ, varied from 16 to 40 ms (^{7}Li) and 2 to 11 ms (^{19}F). For the dstebpgp3s program, the signal attenuation, E, was fit to

$$E = e^{-\gamma^2 g^2 \delta^2 D_i(\Delta - \frac{5\delta}{8} - \tau_d)} \quad (11)$$

where γ is the gyromagnetic ratio, g is the gradient strength, D_i is the self-diffusion coefficient of species i, and τ_d is the delay for gradient recovery. For the stebpgp1s program, the signal attenuation was fit to

$$E = e^{-\gamma^2 g^2 \delta^2 D_i(\Delta - \frac{\delta}{4})}. \quad (12)$$

For both pulse programs, corrections for sine-shaped gradients were included.[41] 32 experiments with varying gradient strength, g, were performed for each diffusion coefficient measurement, always resulting in a linear signal attenuation on the Stejskal-Tanner plot. An example of the Li PFG-NMR data for a diffusion time of 0.1 s is shown in Figure S3, which shows the ln(E) vs $\gamma^2 g^2 \delta^2 D_i(\Delta - \frac{5\delta}{8} - \tau_d)$. All parameters on the x-axis are known, thus the magnitude of the slope is the self-diffusion coefficient of Li, D_{Li}.

3. Results and Discussion

The electrochemical characterization experiments were conducted on C8-DMC/LiFSI mixtures contained within one or more Celgard 2500 separators. Our objective is to extract the properties of the C8-DMC/LiFSI electrolyte from these measurements. The ionic conductivity of the electrolytic phase, κ, is extracted from the raw data using Equation 1, which accounts for the tortuosity of the separator, τ, and the volume fraction of the conducting phase in the separator, ϕ_c . The salt diffusion coefficient of the electrolytic phase, *D*, is extracted from the raw data obtained from restricted diffusion experiments using Equations 6 – 8; only tortuosity affects *D*. The ideal transference number, $t_{+,id}$, is obtained from the raw data with no corrections for the presence of a separator. Obviously, the open circuit potential, *U*, obtained from concentration cells (U-cell) is not corrected for tortuosity or porosity because the U-cell contains only liquids. However, the relationship between the thermodynamic factor and *U* contains a volume fraction correction, given by Equation 10 when values of the salt diffusion coefficient and conductivity obtained from separator/electrolyte systems are used. Similarly, the expression for t_+^0 also contains volume fraction corrections, as shown in Equation 9. Electrolyte properties thus obtained, κ, *D*, $t_{+,id}$, and *U* are plotted as a function of molality in Figures 4a – d.

Figure 4a indicates that at low concentrations, conductivity increases dramatically with increasing salt concentration, going through a shallow maximum of 8.49 x 10^{-5} S/cm at m = 0.94 mol/kg. The maximum concentration studied was m = 1.78 mol/kg (25 wt% LiFSI); the solution with m = 2.31 (30 wt% LiFSI) was phase separated, and the solubility limit was taken as the average between these two molalities, which was m = 2.03.[6] The salt diffusion coefficient of our perfluoroether-based electrolytes, shown in Figure 4b, monotonically decreases with increasing

salt concentration. Over the accessible concentration range, D decreases by about an order of magnitude. It is perhaps worth noting that D in other ether-based solvents follow different behavior. For example, in poly(ethylene oxide)-based electrolytes, D is more or less independent of salt concentration over the same concentration window.[36,37] Figure 4c is a plot of the ideal transference number vs. salt concentration. At the lowest concentration, $t_{+,\mathrm{id}}$ is 0.97 which is remarkably close to unity. If our electrolytes were thermodynamically ideal, the near unity transference number would imply that the cation is much more mobile than the anion. As concentration increases, $t_{+,\mathrm{id}}$ decreases monotonically to a value of 0.67 at m = 1.30. The fact that $t_{+,\mathrm{id}}$ is greater than 0.5 everywhere suggests that the cation is more mobile throughout our concentration window. In conventional liquid electrolytes, $t_{+,\mathrm{id}}$ is generally less than 0.5 at all salt concentrations.[42] A high $t_{+,\mathrm{id}}$ is thought to be a desirable characteristic for electrolytes, as that reduces concentration overpotential. However, this is only true if the electrolyte is thermodynamically ideal. In Figure 4d, the open circuit potential for concentration cells is shown in blue as a function of the natural log of salt molality. The potential equals zero when both sides of the U-cell contain the reference electrolyte (m = 0.60 mol/kg). A polynomial fit to the open circuit potential is shown in solid blue circles, and follows the equation, shown as a solid blue line:

$$U(m) = -1.896(\ln m)^4 - 11.761(\ln m)^3 - 23.298(\ln m)^2 - 32.681\ln m - 12.928. \quad (13)$$

If the solution were thermodynamically ideal, then U would be given by the Nernst potential

$$U(c) = -\frac{RT}{F}\ln\left(\frac{c}{c_{ref}}\right), \quad (14)$$

and Table 1 is used to convert concentrations to molality and c_{ref} = 0.89. The open circles and dashed line in Figure 4d represent the Nernst potential.

The thermodynamic factor, $1 + \frac{dln\gamma_{\pm}}{dln\mathrm{m}}$, calculated using Equation 10 and the data shown in Figure 4, is plotted as a function of concentration in Figure 5. It increases monotonically with salt concentration. The transference number, t_+^0, calculated using Equation 9 and the data shown in Figure 4, is plotted as a function of salt concentration in Figure 6. Interestingly, t_+^0 is negative over the entire experimental window. (At the lowest salt concentration, m = 0.05, our approach indicates that t_+^0 is -10.8. The raw data were relatively noisier at this concentration, probably due to low conductivity.)

In Figure 7, the self-diffusion coefficients of the lithium cation, D_{Li}, and the fluorinated anion, D_{FSI}, measured by PFG-NMR are plotted as a function of salt concentration. These diffusion coefficients are sensitive functions of salt concentrations, decreasing by a factor of 30 over our concentration window. However, the self-diffusion coefficients for both species are approximately the same at all salt concentrations, suggesting that their motion is coupled.

The Nernst-Hartley relation is often used to obtain an overall salt diffusion coefficient from PFG-NMR experiments and is usually defined as:[43-45]

$$D_{NMR} = \frac{2D_{Li}D_{FSI}}{D_{Li} + D_{FSI}} \quad (15)$$

However, it should be noted that Equation 15 is only applicable to dilute electrolytes comprising completely disassociated ions. Figure 8 compares D_{NMR} with D; D is the salt diffusion coefficient measured by restricted diffusion. At the lowest concentration, m = 0.28 mol/kg, the two diffusion coefficients are within experimental error. Both diffusion coefficients decrease monotonically with salt concentration. It is evident that D_{NMR} is a more sensitive function of concentration than D.

Analogous to Equation 15, a transference number based on NMR measurements is usually defined as:

$$t_{+,NMR} = \frac{D_{Li}}{D_{Li} + D_{FSI}}. \quad (16)$$

As was the case with Equation 15, Equation 16 is only applicable to dilute electrolytes comprising completely disassociated ions.

We conclude this section by comparing three different measurements of the transference number. Figure 9 compares shows $t_{+,\mathrm{id}}$ in blue, $t_{+,\mathrm{NMR}}$ in red, and t_+^0 in black. Focusing on the data at m = 0.28 mol/kg, $t_{+,id}$ = 0.89. Based on the value of $t_{+,id}$ alone, one might have concluded that the cation is much more mobile than the anion. However, at m = 0.28 mol/kg, $t_{+,NMR}$ = 0.48, suggesting that the cation and the anion are equally mobile. These two conclusions are clearly inconsistent with each other. Interpretations presented above are only true if the salt had disassociated into Li^+ and FSI^- ions that migrated independently of each other. The inconsistency indicates that the migration of Li+ and FSI- are not independent. The nature of ion motion in our electrolytes is complex and captured by full electrochemical characterization. At m = 0.28 mol/kg, t_+^0 = -1.0. The negative value of t_+^0 implies that when a field is applied to an electrolyte with uniform composition, both the Li^+ and FSI^- are driven to the positive electrode. This can only happen if the solution contains charged clusters such as $[Li(FSI)_2]^-$ in addition to other charged species such as Li^+ and FSI^-. It is possible that the observation that D_{Li} and D_{FSI} measured by PFG-NMR are similar due to the fact that most of the ions are present in the form of clusters. The stark differences between $t_{+,NMR}$, $t_{+,id}$ and t_+^0 are noteworthy. The NMR transference number, $t_{+,NMR}$, is positive and independent of concentration. The ideal

transference number, $t_{+,id}$, is positive and a monotonically decreasing function of concentration. In contrast, the rigorously defined transference number, t_+^0, is negative and an increasing function of concentration, suggesting the presence of ion clusters in all of the electrolytes we studied.

4. Conclusion

We have measured the electrochemical properties of a fluorinated electrolyte comprising LiFSI dissolved in a perfluoroether solvent (C8-DMC). Conductivity, κ, was measured by ac impedance, the salt diffusion coefficient, D, was measured by restricted diffusion, and the transference number based on the ideal solution assumption, $t_{+,id}$, was measured using the steady-state current method. The open circuit potential measured in concentration cells, U, was combined with the three measurements described above to obtain the transference number, t_+^0. The equations used to determine t_+^0 are based on concentrated solution theory of Newman, which is applicable to all electrolytes, whether they are ideal or not. The self-diffusion coefficients of Li and FSI were measured by PFG-NMR, and these results give a third measure of the transference number, $t_{+,NMR}$. If all of the salt molecules were dissociated into free Li+ and FSI-, then the three transference numbers are expected to be identical (within experimental error). The data obtained from LiFSI/C8-DMC mixtures differ qualitatively from this expectation. The rigorously defined transference number, t_+^0, is negative across all salt concentrations, and it increases with increasing salt concentration. In contrast, the ideal transference number, $t_{+,id}$, is positive across all salt concentrations and it decreases with salt concentration. The most surprising result is obtained in the dilute limit at m = 0.28 mol/kg where $t_{+,id}$ = 0.89 which suggests that the electrolyte is a single ion conductor,[7,15] while the rigorously defined transference number, t_+^0, at this concentration is -1.0. It is evident that in fluorinated electrolytes, $t_{+,id}$ does not provide direct insight into the relative contribution of cations to the overall cell current. The NMR-based transference number, $t_{+,NMR}$, is approximately 0.5, independent of salt concentration.

When an electric field is applied to a solution of uniform concentration, comprised of fully dissociated anions and cations, the positive ion will migrate toward the negative electrode and the negative ion will migrate toward the positive electrode. In this case, $t_{+,id}$ and $t_{+,NMR}$, which by definition are always positive, provide insight into the relative mobilities of the dissociated cation and anion. Our measurements of negative t_+^0 imply that applying an electric field in an LiFSI/C8-DMC solution results in the migration of both Li+ and FSI- towards the positive electrode. This implies the presence of charged clusters. Further experimental and theoretical work is needed to quantify the nature of charged (individual ions, triplets, etc.) and uncharged species (ion pairs, quadruplets, etc.) in solution.

Conflicts of interest

There are no conflicts to declare.

Acknowledgements

This work was intellectually led by the Joint Center for Energy Storage Research (JCESR), an Energy Innovation Hub funded by the U.S. Department of Energy (DOE), Office of Science, Basic Energy sciences (BES), under Contract No. DEAC02-06CH11357, which supported both synthesis and characterization work conducted by D.B.S., H.Q.N., and L.S.G., under the supervision of N.P.B. Early work by D.B.S. was supported by the National Science Foundation, grant number 1505669, under the SusChEM initiative. The electrolyte synthesis work was initially established by K.R.O., S.J.M., and J.D.S. who were supported by the Center for Mesoscale Transport Properties, an Energy Frontier Research Center supported by the U.S. Department of Energy, Office of Science, Basic Energy Sciences, under award #DE-SC0012673.

References

1 D. Aurbach, B. Markovsky, A. Shechter, Y. Ein-Eli and H. Cohen, *J. Electrochem. Soc.*, 1996, **143**, 3809–3820.

2 R. Fong, U. von Sacken and J. R. Dahn, *J. Electrochem. Soc.*, 1990, **137**, 2009–2013.

3 D. Guyomard and J. M. Tarascon*, J. Electrochem. Soc.*, 1993, **140**, 3071–3081.

4 J. M. Tarascon and D. Guyomard, *Solid State Ionics*, 1994, 69, 293–305.

5 J. H. Baik, D. G. Kim, J. H. Lee, S. Kim, D. G. Hong and J. C. Lee, *J. Ind. Eng. Chem.*, 2018, **64**, 453–460.

6 D. B. Shah, K. R. Olson, A. Karny, S. J. Mecham, J. M. DeSimone and N. P. Balsara, *J. Electrochem. Soc.*, 2017, **164**, A3511–A3517.

7 M. Chintapalli, K. Timachova, K. R. Olson, S. J. Mecham, D. Devaux, J. M. Desimone and N. P. Balsara, *Macromolecules*, 2016, **49**, 3508–3515.

8 D. H. C. Wong, J. L. Thelen, Y. Fu, D. Devaux, A. A. Pandya, V. S. Battaglia, N. P. Balsara and J. M. DeSimone, *Proc. Natl. Acad. Sci.*, 2014, **111**, 3327–3331.

9 Z. Zhang, L. Hu, H. Wu, W. Weng, M. Koh, P. C. Redfern, L. A. Curtiss and K. Amine, *Energy Environ. Sci.*, 2013, **6**, 1806–1810.

10 E. Markevich, G. Salitra, A. Rosenman, Y. Talyosef, F. Chesneau and D. Aurbach, *Electrochem. Commun.*, 2015, **60**, 42–46.

11 R. McMillan, H. Slegr, Z. X. Shu and W. Wang, *J. Power Sources*, 1999, **81**, 20–26.

12 Y.-M. Lin, K. C. Klavetter, P. R. Abel, N. C. Davy, J. L. Snider, A. Heller and C. B. Mullins, *Chem. Commun.*, 2012, **48**, 7268–7270.

13 J. Newman and K. E. Thomas-Alyea, *Electrochemical Systems*, John Wiley & Sons, Inc., Hoboken, New Jersey, 2004.

14 Y. Ma, M. Doyle, T. F. Fuller, M. M. Doeff, L. C. De Jonghe and J. Newman, *J. Electrochem. Soc.,* 1995, **142**, 1859–1868.

15 R. Berger, G. Resnati, P. Metrangolo, E. Weber and J. Hulliger, *Chem. Soc. Rev.*, 2011, **40**, 3496–3508.

16 J. A. Gladysz, D. P. Curran and I. T. Horvath, *Handbook of Fluorous Chemistry*, Wiley Online Library, Weinheim, Germany, 2004.

17 I. Villaluenga, K. H. Wujcik, W. Tong, D. Devaux, D. H. C. Wong, J. M. DeSimone and N. P. Balsara, *Proc. Natl. Acad. Sci. U. S. A.*, 2015, **113**, 52–57.

18 L. O. Valøen and J. N. Reimers, *J. Electrochem. Soc*., 2005, **152**, A882–A891.

19 A. Nyman, Mårten Behm and G. Lindbergh, *Electrochim. Acta.*, 2008, **53**, 6356–6365.

20 J. Evans, C. A. Vincent and P. G. Bruce, *Polymer*, 1987, **28**, 2324–2328.

21 P. G. Bruce and C. A. Vincent, *J. Electroanal. Chem.*, 1987, **225**, 1–17.

22 A. Noda, K. Hayamizu and M. Watanabe, *J. Phys. Chem. B*, 2001, **105**, 4603–4610.

23 M. Gouverneur, F. Schmidt and M. Schönhoff, *Phys. Chem. Chem. Phys.*, 2018, **20**, 7470–7478.

24 K. Timachova, M. Chintapalli, K. R. Olson, S. J. Mecham, J. M. DeSimone and N. P. Balsara, *Soft Matter*, 2017, **13**, 5389-5396.

25 H. G. Buss, S. Y. Chan, N. A. Lynd and B. D. McCloskey, *ACS Energy Lett.*, 2017, **2**, 481–487.

26 M. Joost, M. Kunze, S. Jeong, M. Schönhoff, M. Winter and S. Passerini, *Electrochim. Acta*, 2012, **86**, 330–338.

27 K. R. Olson, D. H. C. Wong, M. Chintapalli, K. Timachova, R. Janusziewicz, W. F. M. Daniel, S. Mecham, S. Sheiko, N. P. Balsara and J. M. DeSimone, *Polymer*, 2016, **100**, 126–133.

28 J. Landesfeind, J. Hattendorff, A. Ehrl, W. A. Wall and H. A. Gasteiger, *J. Electrochem. Soc.*, 2016, **163**, A1373–A1387.

29 D. Devaux, Y. H. Chang, I. Villaluenga, X. C. Chen, M. Chintapalli, J. M. Desimone and N. P. Balsara, *J. Power Sources*, 2016, **323**, 158–165.

30 D. M. Pesko, M. A. Webb, Y. Jung, Q. Zheng, T. F. Miller, G. W. Coates and N. P. Balsara, Macromolecules, 2016, 49, 5244–5255.

31 J. Newman and T. W. Chapman, *AIChE J.*, 1973, **19**, 343–348.

32 A. Ehrl, J. Landesfeind, W. A. Wall and H. A. Gasteiger, *J. Electrochem. Soc.*, 2017, **164**, A826–A836.

33 S. D. Thompson and J. Newman, *J. Electrochem. Soc.*, 1989, **136**, 3362–3369.

34 S. Stewart and J. Newman, *J. Electrochem. Soc.,* 2008, **155**, A458–A463.

35 N. P. Balsara and J. Newman, *J. Electrochem. Soc.*, 2015, **162**, A2720–A2722.

36 I. Villaluenga, D. M. Pesko, K. Timachova, Z. Feng, J. Newman, V. Srinivasan and N. P. Balsara, *J. Electrochem. Soc.*, 2018, **165**, A2766–A2773.

37 D. M. Pesko, K. Timachova, R. Bhattacharya, M. C. Smith, I. Villaluenga, J. Newman and N. P. Balsara, *J. Electrochem. Soc.*, 2017, **164**, E3569–E3575.

38 A. Ehrl, J. Landesfeind, W. A. Wall and H. A. Gasteiger, *J. Electrochem. Soc.*, 2017, **164**, A2716–A2731.

39 J. Alexej and M. Norbert, *J. Magn. Reson.*, 1997, **375**, 372–375.

40 K. M. Diederichsen, K. D. Fong, R. C. Terrell, K. A. Persson and B. D. McCloskey, *Macromolecules*, 2018, **51**, 8761–8771.

41 D. Sinnaeve, *Concepts Magn. Reson. Part A*, 2012, **40A**, 39–65.

42 D. Devaux, R. Bouchet, D. Glé and R. Denoyel, *Solid State Ionics*, 2012, **227**, 119–127.

43 V. K. Vanag and I. R. Epstein, Phys. Chem. Chem. Phys., 2009, **11**, 897–912.

44 J. Barthel, H. Krienke, W. Kunz, *Physical chemistry of electrolyte solutions*, Steinkopff, Darmstadt, 1998.

45 G. S. Hartley, *Philos. Mag.*, 1931, **12**, 473.

Nomenclature

A	Active surface area of electrode (cm^2)
a, b	Fit parameters in Equation 5
$\boldsymbol{c}$	Concentration (mol/L)
$\boldsymbol{D}$	Salt diffusion coefficient of electrolytic phase (cm^2/s)
$\boldsymbol{D_i}$	Self-diffusion coefficient of species i as measured by PFG-NMR (cm^2/s)
$\boldsymbol{D_{FSI}}$	Self-diffusion coefficient of FSI as measured by PFG-NMR (cm^2/s)
$\boldsymbol{D_{Li}}$	Self-diffusion coefficient of Li as measured by PFG-NMR (cm^2/s)
$\boldsymbol{D_{NMR}}$	Overall self-diffusion coefficient (cm^2/s)
$\boldsymbol{D_s}$	Salt diffusion coefficient of electrolyte in separator (cm^2/s)
E	Attenuation of the echo
$\boldsymbol{F}$	Faraday's constant (96,485 C/mol)
G	Gradient strength
I_{ss}	Steady-state current (mA)
I_o	Initial current (mA)
k_0	Offset voltage (mV)
L_c	Inductance of measurement cabling (H)
l	Thickness of electrolyte/separator (cm)
$\boldsymbol{m}$	Molality (mol/kg)
N_m	MacMullin number; obtained by taking the ratio of κ/κ_s
Q_{el}	Constant phase element of the electrolyte
Q_{int}	Constant phase element of the interface
R	Ideal gas constant (J/mol K)
R_c	Resistance of measurement cabling (Ω)
R_{int}	Resistance of electrolyte/electrode interface (Ω)
$R_{i,0}$	Resistance of electrolyte/electrode interface initially, prior to polarization (Ω)
$R_{i,ss}$	Resistance of solvent/electrode interface when I_{ss} reached (Ω)
R_s	Resistance of electrolyte/separator composite (Ω)
R_T	Total resistance of cell ($R_s + R_{i,0}$)
T	Temperature (K)
T_f	Thermodynamic factor
t	Time (s)
$\boldsymbol{t_+^0}$	Transference number obtained using the Balsara and Newman method
$\boldsymbol{t_{+,id}}$	Ideal transference number using steady-state current method
$t_{+,NMR}$	Transference number obtained using pulsed field gradient NMR
$\boldsymbol{U}$	Open-circuit voltage (mV)
$\boldsymbol{z^+}$	Cation charge
$\boldsymbol{1 + \frac{dln\gamma_\pm}{dlnm}}$	Thermodynamic factor

Greek

$\boldsymbol{\alpha}$	Nondimensional time
$\boldsymbol{\gamma}$	Gyromagnetic ratio
$\boldsymbol{\gamma_{\pm}}$	Mean molal activity coefficient of the salt
$\boldsymbol{\Delta}$	Diffusion interval (s)
$\boldsymbol{\Delta V}$	Dc polarization potential (mV)
$\boldsymbol{\delta}$	Length of gradient pulse (s)
$\boldsymbol{\kappa}$	Conductivity of the electrolytic phase; (S/cm)
$\boldsymbol{\kappa_s}$	Conductivity of the electrolyte and separator combined; (S/cm)
$\boldsymbol{v}$	Stoichiometric parameter = 2 for univalent salts ($= v^+ + v^-$)
$\boldsymbol{v^i}$	Number of cations/anions per molecule of salt ($i = +$ or $-$)
$\boldsymbol{\rho}$	Density of electrolyte (g/L)
$\boldsymbol{\tau}$	Tortuosity of the separator
$\boldsymbol{\tau_d}$	Delay for gradient recovery (s)
$\boldsymbol{\phi_c}$	Volume faction of conducting phase in separator

Figures

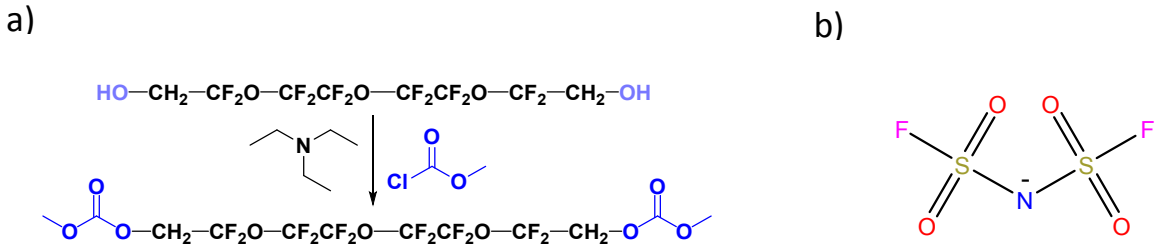

Figure 1: (a) Reaction to produce C8-DMC from the commercial C8-Diol analog and (b) FSI anion.

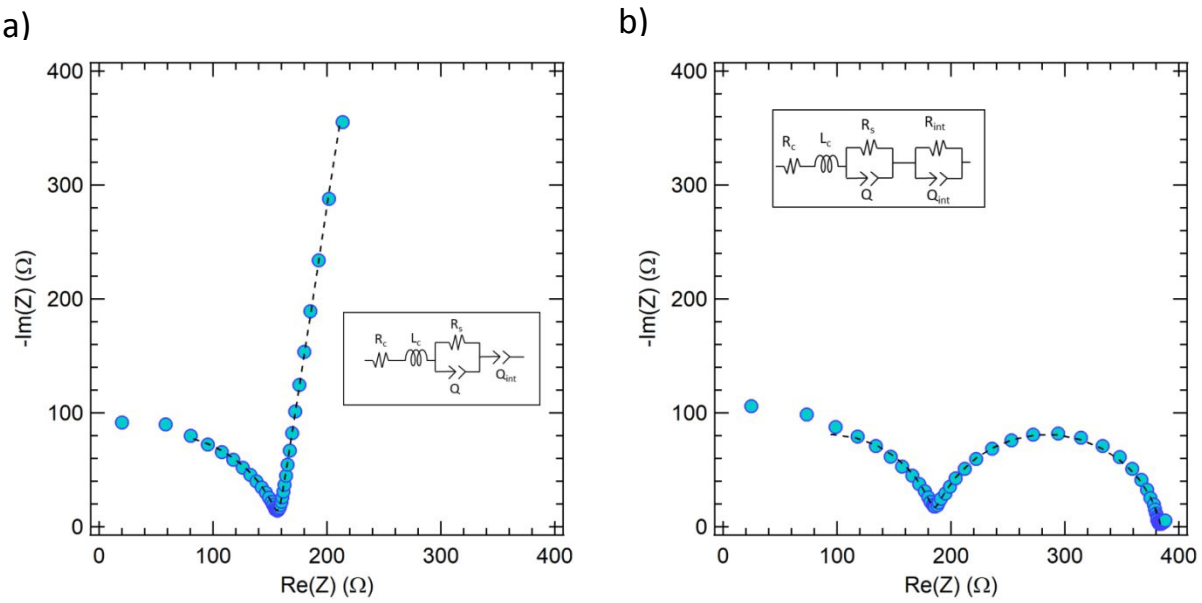

Figure 2: Ac impedance data of C8-DMC/LiFSI at *m* = 0.60 mol/kg at T = 30 °C. (a) A symmetric cell with stainless steel (blocking) electrodes (data shown to 250 Hz for clarity) and (b) a symmetric cell with lithium (non-blocking) electrodes. The dashed black lines are fits to the equivalent circuits shown.

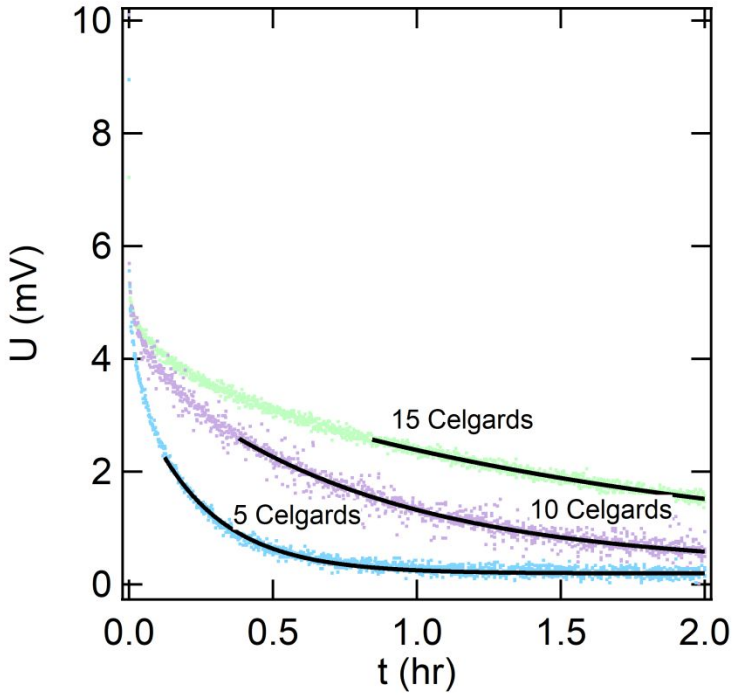

Figure 3: Open circuit potential versus time after dc polarization of 40 mV of a C8-DMC/LiFSI electrolyte with m = 0.60 mol/kg in lithium-electrolyte-lithium cells with Celgard 2500 separators. The number of Celgard 2500 separators was varied to obtain different electrolyte thicknesses. Salt diffusion coefficients are extracted by fitting the data to Equation 5 (solid black curves). The diffusion coefficients obtained from the different fits are in good agreement (1.86 x 10^{-8} (α = 0.051), 2.39 x 10^{-8} (α = 0.051), 2.39 x 10^{-8} (α = 0.050) cm^2/s for 5, 10 and 15 stacked Celgards, respectively).

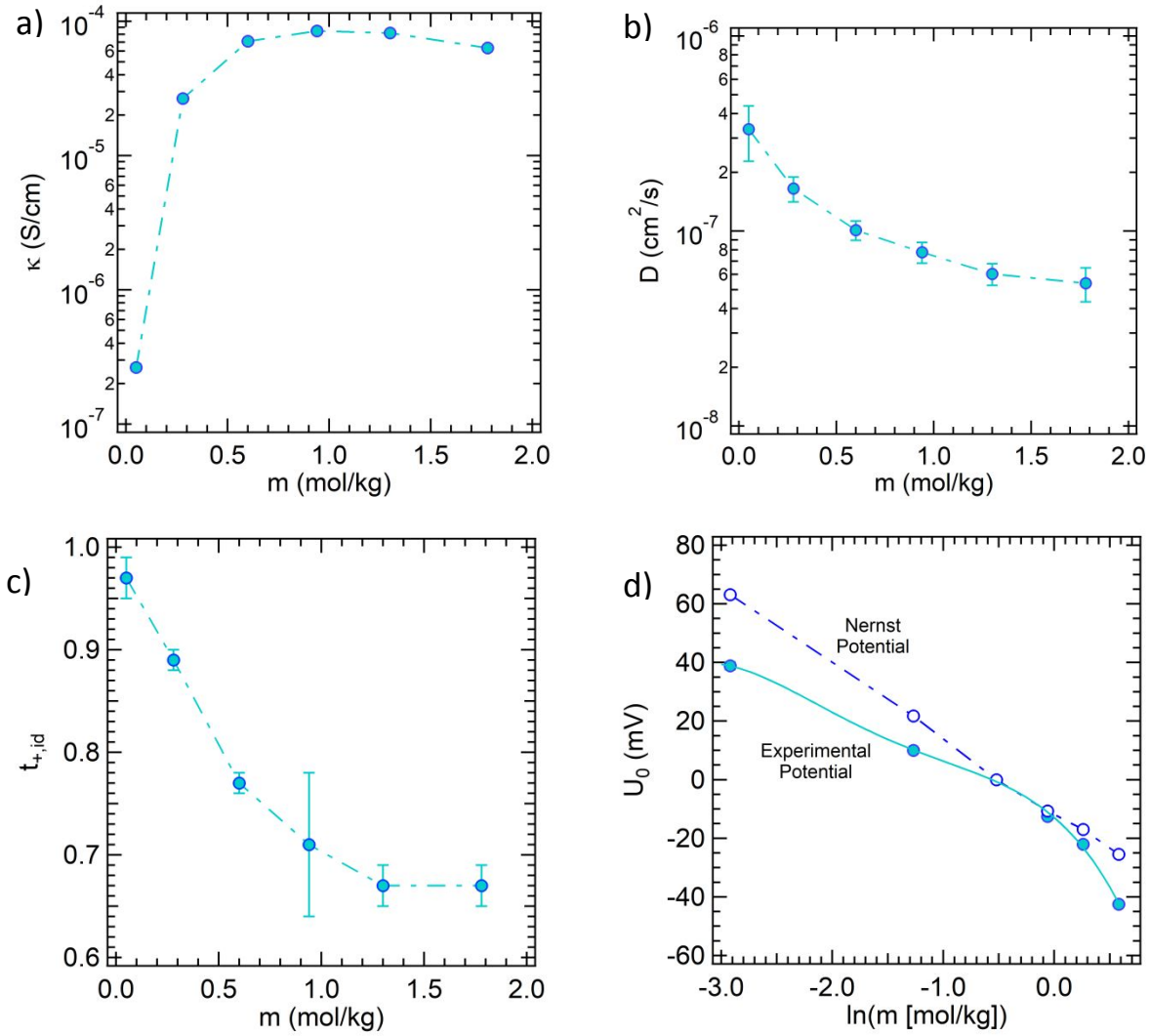

Figure 4: Electrochemical properties of C8-DMC/LiFSI (electrolytic phase) as a function of molality. **(**a) The conductivity measured by ac impedance, (b) the diffusion coefficient measured by the restricted diffusion method, and (c) $t_{+,id}$ as measured by the steady-state current method. d) Results obtained in concentration cells with $m_{\mathrm{ref}} = 0.60$ mol/kg (solid symbols). The solid line is a fit through the experimental data (Eqn. 13). The open symbols and dashed line give the Nernst potential (Eqn. 14).

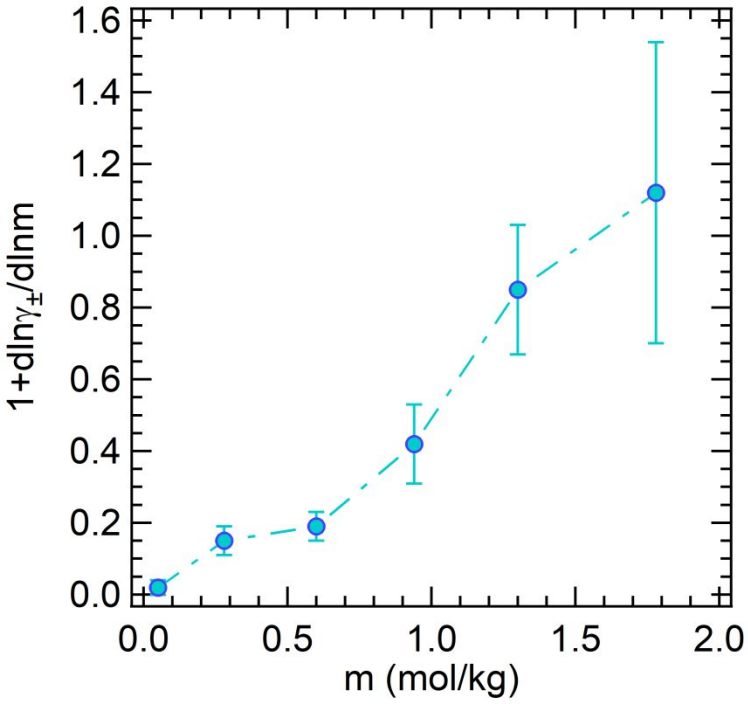

Figure 5: The thermodynamic factor as a function of salt concentration

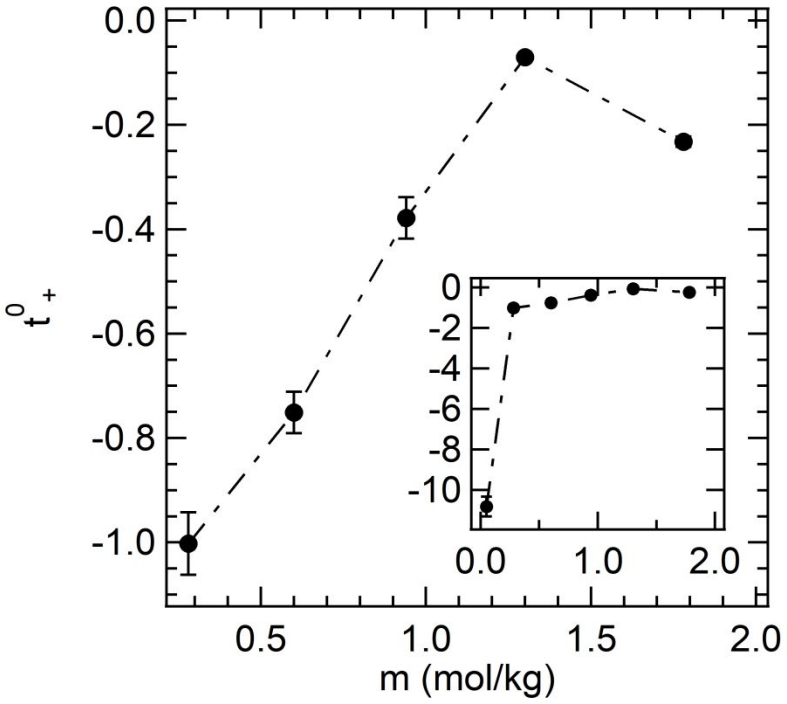

Figure 6: Transference number, t_+^0, based on concentrated solution theory as a function of salt concentration in the range m = 0.28 to 1.78 mol/kg. The inset includes data at a very low concentration, m = 0.05 mol/kg. The rest of the paper will focus on the range m = 0.28 to 1.78 mol/kg

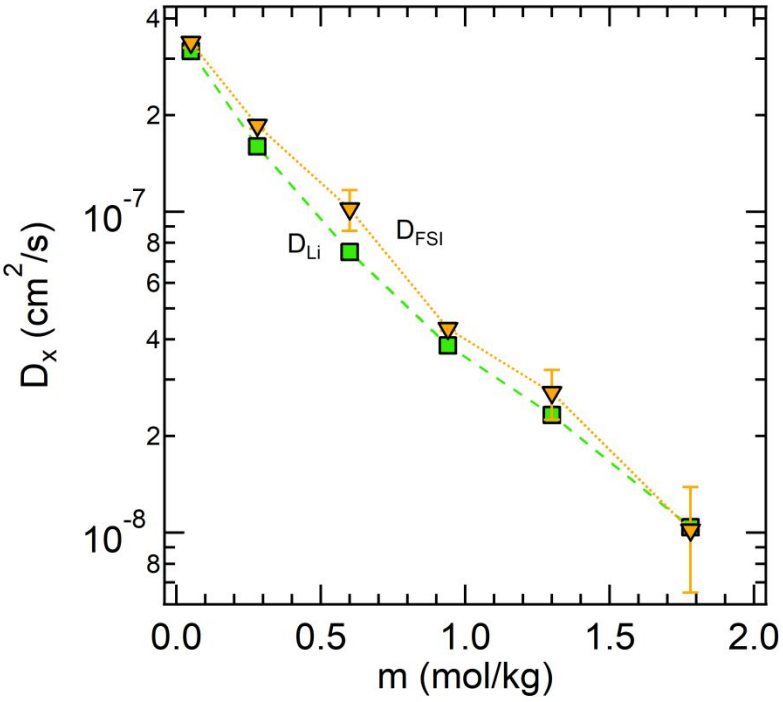

Figure 7: Self-diffusion coefficients of Li and FSI determined by PFG-NMR as a function of salt concentration. D_{FSI} and D_{Li} are very similar throughout the concentration window.

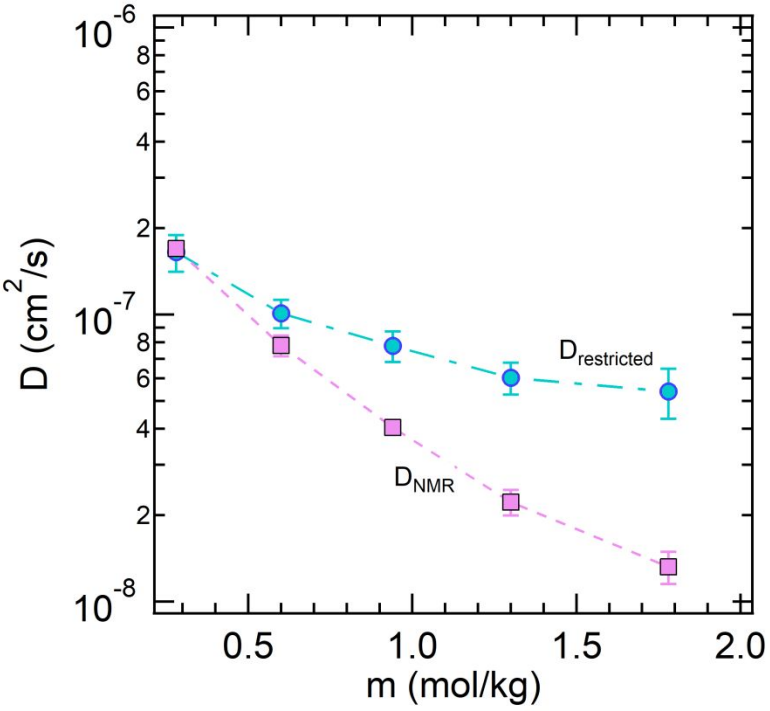

Figure 8: Dependence of the salt-diffusion coefficients measured by PFG-NMR and restricted diffusion on salt concentration.

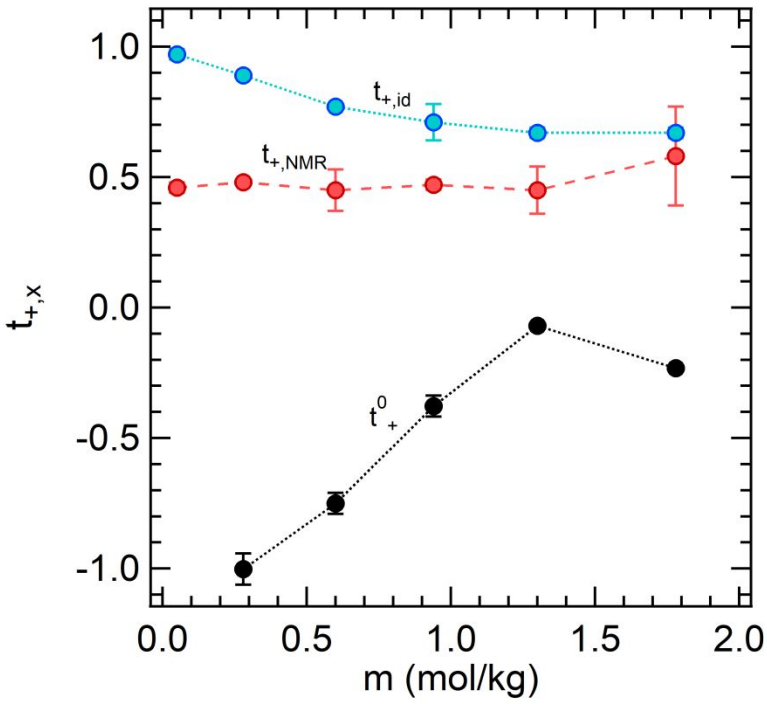

Figure 9: The cation transference numbers measured by the steady-state current method, $t_{+,id}$, and PFG-NMR, $t_{+,NMR}$, are compared with the rigorously defined transference number based on concentrated solution theory, t_+^0, at different salt concentrations. The lack of agreement between the three measurements indicates the presence of ion clusters

Tables

Table 1: Values of LiFSI wt %, molality, calculated concentration, and measured density for C8-DMC electrolytes

LiFSI wt%	*m* (mol/kg)	*c* (mol/L)	ρ (g/L)
0	0	0	1459 ± 64
1.0	0.05	0.08	1487 ± 26
5.0	0.28	0.39	1447 ± 72
10.0	0.60	0.89	1660 ± 17
14.9	0.94	1.36	1681 ± 24
19.6	1.30	1.70	1627 ± 75
25.0	1.78	2.36	1764 ± 14

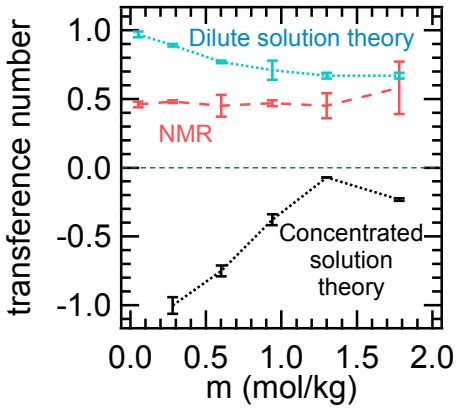

Flourinated electrolytes are highly non-ideal and Newman's concentrated solution theory must be used to fully characterize ion-transport.